Materials Today: Proceedings 70 (2022) 321–327

Contents lists available at ScienceDirect

Materials Today: Proceedings

journal homepage: www.elsevier.com/locate/matpr

3D printing of polyvinylidene fluoride composite films with enhanced electroactive beta-phase for flexible wearable pressure sensors

K.B. Mustapha *, Khaled Mohamed Metwalli, Ab Aziz Bin Baharuddin, Yousif Abakr

Department of Mechanical, Materials and Manufacturing Engineering, University of Nottingham (Malaysia Campus), 43500 Semenyih, Malaysia

ARTICLE INFO

Article history:
Available online 24 September 2022

Keywords:
PVDF-HFP
Fused deposition modelling
Piezoelectric polymer
Solvent evaporation casting
Barium titanate
Activated carbon

ABSTRACT

Following the notable rise of three-dimensional (3D) printing in recent years, its use for the fabrication of functional devices derived from piezoelectric polymers such as poly (vinylidene fluoride), PVDF, has become an active area of research. However, there is still a lot to understand about the structure–property-processing relationship regarding the 3D printing of PVDF-based polymers with an enhanced piezoelectric property, which is closely related to the β-phase crystal structure of the polymer. This paper presents the preliminary results of investigations into the extrusion-based 3D printing of poly(vinylidene fluoride-hexafluoropropylene), PVDF-HFP, a PVDF copolymer. Towards the enhancement of the β-phase content of this copolymer, the study analyzed the influence of two fillers in the form of barium titanate ($BaTiO_3$) and untreated activated carbon (UAC) and considered the effect of two printing parameters on the piezoelectric crystalline structure of the PVDF-HFP. First, composite films of the PVDF-HFP with the fillers were formed via the solvent evaporation casting method. From the characterization of the solvent-cast samples using Fourier Transform Infrared Spectrum (FTIR), a composite consisting of 10.55 wt% $BaTiO_3$ and 0.45 wt% UAC with the matrix of PVDF-HFP was found to produce a superior β-phase content (67%) and it was deployed for syringe-based extrusion-assisted 3D printing. Post-fabrication characterization of the extruded samples was carried out to examine the influence of the 3D printing conditions in the form of printing bed temperature (50, 75, 95) and extrusion speed (10, 15, 25). It was found that the combination of a higher printing bed temperature and a low printing speed further enhanced the β-phase content for the PVDF-HFP composites, yielding a β-phase content of 79.6%. Confirmation of the electromechanical/piezoelectric response of the unpoled strips of printed samples revealed a positive correlation between the externally applied pressure on the printed strips and generated voltage.

Selection and peer-review under responsibility of the scientific committee of The International Conference on Additive Manufacturing for a Better World.

1. Introduction

Fabrication of smart materials was once dominated by expensive and energy-intensive techniques that include lithography, hot pressing/embossing, spin coating, electrospraying, cryogenic ball milling, and Langmuir-Blodgett deposition, among others [1]. However, with the huge demand for low-cost, complex-yet-flexible intelligent components across industries, a continuous search exists for inexpensive methods suitable for the production of functional components from stimuli-responsive materials [2,3]. Such smart components have ample applications for personal electronics, energy devices, wearable implantable sensors, biomedical-related assistive devices such as haptics, artificial muscles, and drug delivery systems [4]. In recent years, researchers have become bullish on the role of additive manufacturing (AM) or three-dimensional (3D) printing platforms towards the broader objectives of facilitating the production of an assortment of smart devices with intricate 3D shapes [5].

Overall, 3D printing platforms [3,6]: (i) allow the production of wider freeform designs from different types of materials ranging

Abbreviations: FDM, Fused deposition modelling; PVDF-HFP, Poly(vinylidene fluoride-hexafluoropropylene); PVDF, Poly (vinylidene fluoride); MEAM, Material extrusion AM; PVDF-TrFE, Polyvinylidene fluoride-trifluoroethylene; DOE, Design of Experiment.

* Corresponding author.
E-mail address: KhameelB.Mustapha@nottingham.edu.my (K.B. Mustapha).

https://doi.org/10.1016/j.matpr.2022.09.245

Selection and peer-review under responsibility of the scientific committee of The International Conference on Additive Manufacturing for a Better World.

from metals, polymers, ceramics, and composites; (ii) facilitate the creation of multi-material/multifunctional devices within a single production space; and (iii) enable the tailoring of complex spatial distribution of mechanical/thermal/chemical/electrical properties. From the survey of related literature, three crucial factors essential to accelerating the maturity of AM technology are identified as processing methodologies, printing machines and printing materials [7]. On the methodologies and machine fronts, significant strides have been recorded concerning various subsets of AM protocols that range from binder jetting, vat photo-polymerization, powder bed fusion, material extrusion, material jetting, directed energy deposition, to sheet lamination [3,8]. Overall, each of these AM processes favor a limited class of materials, and they each have pros and cons as pinpointed by Ligon et al [7]. Nevertheless, bolstered by its ease of scalability and the proliferation of inexpensive fabrication platforms, the material extrusion AM (MEAM) technology has gained substantial popularity among the methods that employ polymer-based materials over the past decades [9]. On the one hand, FDM has enabled the fast digital fabrication of integrated polymeric smart structures and flexible electronics using two major clusters of smart materials (e.g., shape memory polymers and piezoelectric polymers) as captured in various reviews [2,10]. On the other hand, the pure form of these smart polymer material feedstocks typically needs various forms of improvements to meet the increasing demand for enhanced functionality across application domains.

Catering to the above challenge, an extensive body of work has emerged that paired the simplicity of FDM with the processing of smart polymeric materials. It is worth noting that only a few of these smart polymers exist (e.g. shape memory polymers and piezoelectric polymers), largely because of the constraint of controlled conditions required for their processing. Owing to critical applications in energy harvesting, intelligent soft robots, wearable medical sensing, defence/aerospace/automotive structural health monitoring purposes, piezoelectric polymers based on poly (vinylidene fluoride) (PVDF) and its copolymers have caught the attention of researchers for the production of functional devices using FDM [2,10,11]. Analogous to their inorganic ceramic-based counterparts such as Lead Zirconate Titanate (PZT), when piezoelectric polymers are strained, they generate electricity under the right set of conditions. And conversely, when an electric field is applied to them, they are mechanically stressed. However, unlike PZT, fluoroplastics such as PVDF are less toxic and are better suited for flexible sensing applications [12].

A brief highlights of the observations from a short collection of important studies at the intersection of PVDF and FDM is provided next. Broadly, three categories of studies can be identified. At one end are studies that focused on the FDM fabrication of pure PVDF. This can be seen in the works of Lee and Tarbutton [13], Porter *et al* [14] and Momenzadeh *et al* [15], and Fan *et al* [16]. A major feature of these studies is the requirement for external poling of the FDM-produced samples. The poling process, which is done either *in-situ* or after fabrication with FDM, is needed to create dipole alignment of the polymer and requires an elaborate set-up with a prohibitive high voltage that ranges from $1MV/m$ - $130MV/m$ [17]. The necessity for this poling arises from the fact that PVDF and its copolymers exhibit polymorphism that leads to the existence of five crystalline phases ($\alpha, \beta, \gamma, \delta, \varepsilon$) [18]. Of all these phases, the α crytal phase is the most kinetically stable that formed easily during most processing techniques. But this phase is nonpolar, generally lacks piezoelectric effect, and it is mostly used for insulating applications [19]. In contrast, the β crystal phase has an orthorhombic structure and exhibits the desired piezoelectric behavior among all five phases. Notably, transforming from the α-phase to the β-phase (depicted in Fig. 1) requires huge mechanical stretching/thermal treatment and/or contact/corona poling.

A substantive question that then arises is "how to produce PDVF-based functional devices with minimal or no poling requirement"?. Towards answering this question, another category of studies has sought the use of composites of PVDF with fillers in the form of barium titanate, carbon nanotubes, zinc oxide, etc. A few related studies in this group include the work by Kim *et al* [20] (extruder-based FDM with in-situ poling), Bodkhe *et al* [21] (poling via ball milling), Kumar *et al* [22] (absence of a piezoelectric test, hence no poling done), and Sharma *et al* [23] (absence of a piezoelectric test, hence no poling done). Yet, while the prudent use of these fillers has been found useful, the proportion of the β-phase often remains low (40 – 55 %) without additional poling. The current investigation falls within the third category of a rather small number of studies that seek improvement in the synthesis of the β-phase by employing the copolymers of PVDF and their composites within the framework of extrusion-based 3D printing [24,25]. The two common copolymers that have received the attention of researchers so far are polyvinylidene fluoride-trifluoroethylene (PVDF-TrFE) and polyvinylidene fluoride-hexafluoropropylene (PVDF-HFP). Specifically, Marandi and Tarbutton [26] reported the FDM fabrication of PVDF-TrFE (supplemented by corona poling) and Ikei *et al* [27] also presented a similar study with in-situ 3D printing and poling. In contrast, the present work is devoted to the production of electroactive structures based on the composites of PVDF-HFP using a syringe-based FDM process. We pursued the impacts of processing and composition of fillers in the form of barium titanate and activated carbon on the enhancement of the β-phase content of PVDF-HFP. To the best of our knowledge, this represents the first such study within the framework of enhancement of the β-phase in additively-manufactured PVDF copolymer structures.

The rest of the paper is structured as follows. Section 2 details the materials and methods employed in this study. Section 3 presents a brief discussion of the results, while section 4 contains the concluding remarks.

2. Materials and methods

2.1. Materials

The four materials involved in this study are: (i) the polymer matrix in the form of polyvinylidene fluoride-hexafluoropropylene (PVDF-HFP); (ii) fillers in the form of perovskite structured nanoparticles of barium titanate and an untreated activated carbon (UAC); and (iii) dimethyl sulfoxide (DMSO). The PVDF-HFP was obtained in form of pellets, while $BaTiO_3$ (BTO) is received in the form of powder, both were purchased from Sigma-Aldrich. The UAC and DMSO were sourced from EvaChem and chemAR, respectively. Table 1 contains some basic properties of the materials.

2.2. Methods

Fig. 2 illustrates the key stages of the methodology employed in this study. The first stage involves the preparation of PVDF-HFP composite films via the solvent evaporation casting method. This is done to study the effect of various weight fractions of the fillers on the crystalline structure of the PVDF-HFP. One of the strategic importance in our choice of PVDF-HFP is that it is cheaper than the pure PVDF and soluble in environmentally friendly solvents such as DMSO as first reported by Aldas *et al* [28]. It is worthy of note that, in virtually all previous studies involving FDM and PVDF/PVDF copolymers, mostly protic solvents such as *N*,*N*-dimethylformamide (DMF) and Dimethylacetamide (DMA) are used in combination with acetone and DMSO. However, the cur-

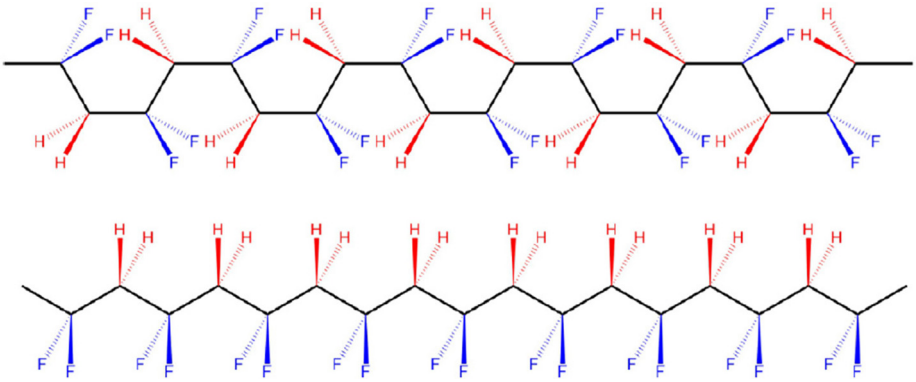

Fig. 1. Schematic of the α crystalline phase (top) and the β crystalline phase (bottom)[18].

Table 1
Basic properties of the materials.

Materials	Properties	
PVDF-HFP	Melting temperature	140–145 °C
	Density	1.75 g at 25 °C
	Melt flow rate	3.5–7.5 g/10 min (230 °C/12.5 kg)
DMSO	Purity	99.9 % pure
	Boiling point	189 °C
	Density	1.1 g/cm^3
	Flashpoint	87 °C
$BaTiO_3$	Purity	99 %
	Appearance	White
	Density	6.08 g/mL at 25 °C
UAC	Appearance	Black
	Density	1.48 g/cm^3

Table 2
Experimental runs based on extreme vertices mixture design of experiment.

Sample	PVDF-HFP	BTO	UAC
A	98	0	2
B	85	15	0
C	83	15	2
D	99.5	0	0.5
E	99.5	0.5	0
F	93	6.1	0.9
G	95.5	3.05	1.45
H	89	10.55	0.45
I	88	10.55	1.45
J	96.25	3.05	0.7
K	96.25	3.3	0.45

rent study explored the conditions that allow the complete dissolution of the PVDF-HFP pellets solely in DMSO with no other solvent. This provides the added advantage of making the films derived from this study far less toxic than other studies.

2.2.1. Fabrication of films

For the films, 2.25 g of PVDF-HFP pellets were dissolved in 20*ml* of DMSO for 2 h at 85 °C (5 °C less than that stated in [29]). After the full dissolution of the pellets, proportions of the $BaTiO_3$ and the UAC were subsequently added. The as-prepared solution of PVDF-HFP-BTO-UAC is then subjected to vigorous magnetic stirring for 10 min and then dried on a glass substrate in an oven for 15 h at 100 °C. The oven-drying step completely removes the DMSO from the film of various composites. For a systematic discovery of how the volume fractions of the fillers influence the crystal phase of the films, the mixture design of the experiment (MDOE) is adopted [30]. Technically, the MDOE, unlike the conventional DOE, provides an efficient experimental design framework for situations where the independent factors exist as proportions of different components of a blend that must add up to 100 %, as we have here [30]. The *Extreme-Vertices* type of MDOE tool in Minitab® is employed to arrive at the combination shown in Table 2.

The solution evaporation casting method is used to produce film samples based on the material proportions listed in Table 2. Subsequently, the β-phase content of the produced films are characterized using Fourier transform infrared spectroscopy (FTIR). For the FTIR, a PerkinElmer FTIR spectrometer was employed to scan and obtain the vibrational spectra of all samples based on the wavelength range of 600 and 1400 cm^{-1} [20]. From the scans, the percentage of absorbance was measured and plotted against the wavelength. Further, the percentage of the β-phase content was also determined using the Beer-Lambert Law [31].

2.2.2. Additive manufacturing of samples and post-fabrication tests

After determining the solution-cast composite combination with the best β-phase content via the FTIR characterizations of the specimen produced based on Table 2, a composite gel of the PVDF-HFP-BTO-UAC is derived for onward use with a syringe-

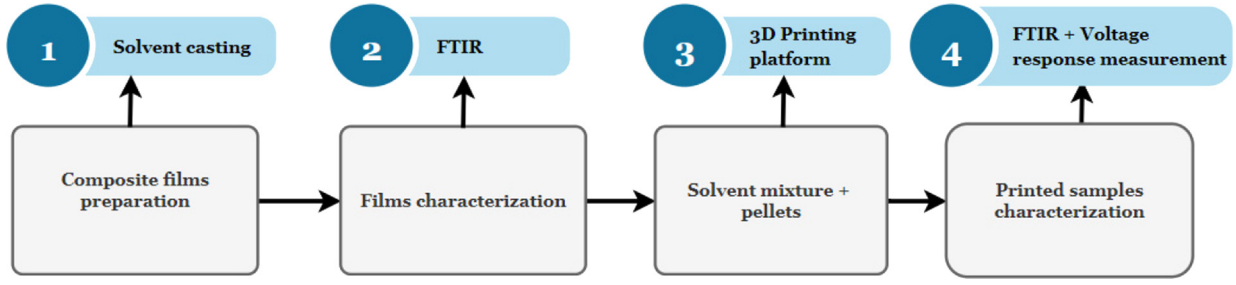

Fig. 2. An illustration of the methodological steps.

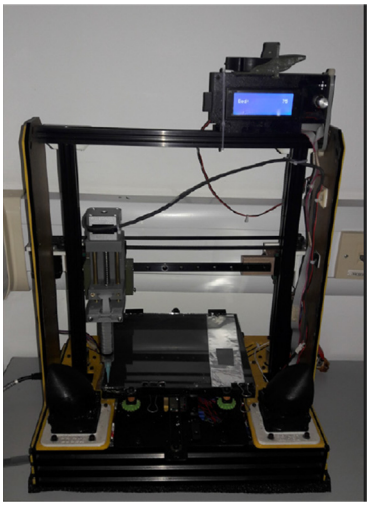

Fig. 3. A syringe-based FDM platform with strips of films printed on aluminium foil.

based fused deposition modelling (FDM) platform shown in Fig. 3. It is worth pointing out that pellets of the composite were also derived and then used for filament formation in a filament-based FDM platform. However, for brevity's sake, the presentation here is limited to results from the syringe-based FDM process. Procedurally, the working mechanism of the syringe-based printing platform employs the frame and software of a modified commercial 3D printer (Prusa). This allows the control of some key printing variables such as the nozzle temperature, printing bed temperature, printing speed etc. For this study, the printing speed and the printing bed temperature are varied to further investigate their influence on the β-phase content and pressure sensing responseof the printed sample. All printing samples were produced with a longitudinal printing direction. Table 3 shows the non-mixture traditional DOE table employed to guide the fabrication of specimens for the post-fabrication characterization and tests.

Based on the general full factorial DOE, Table 3 leads to a total of 9 experimental runs (3^2), and consequently, 9 samples were additively manufactured. FTIR characterization is then conducted on the samples to re-assess the β-phase content. Next, to address the impact of the FDM printing conditions on the electromechanical response, the open circuit voltage generated by the AM-produced samples under the application of external pressure is measured. For the test, aluminium foil was applied on both sides of the printed samples to act as electrodes. Employing a set-up similar to the one in [32], the electrode samples were housed in an enclosure with an opening connected to a portable air pump pedal inflator with pressure readings. For voltage reading, wires connected to the top and bottom electrodes on the printed composite strips were then connected to a multimeter.

3. Results and discussion

This section presents a brief discussion of the selected results from the study. Mostly, the effects of the filler contents and the FDM printing conditions are highlighted. Fig. 4 shows representative images of the oven-dried solution-cast films within a glass petri dish. Samples F, G, H, and I, previously listed in Table 2, are shown in this image to reveal the change in appearance with the various weight fractions of the fillers. As would be observed, the appearance changed from light grey in sample H (10.55 wt% BTO against the 0.45 wt% UAC content), grey (samples of I and F) to darkish grey in sample G (with 3.05 wt% BTO vs the 1.45 wt% UAC).

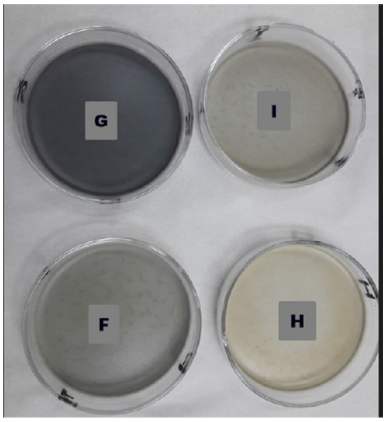

Fig. 4. Oven-dried solution-cast samples.

For brevity's sake, Fig. 5 compares the variation of the recorded FTIR spectra for four selected samples (A, B, C and H) listed in Table 2. The spectra shows the variation in the infrared (IR) absorption bands for: (i) Sample A containing PVDF-HFP and UAC only; (ii) Sample B containing PVDF-HFP and BTO only; (iii) Sample C, containing the maximum weight fractions of BTO and UAC considered; and (iv) Sample H comprising the composition that yields the highest β-phase content when both BTO and UAC are present in the composite film. From past studies, the various absorption bands that correspond to the α-phase of PVDF and its copolymers were identified as 614, 766, 795, 855, and 976 cm^{-1}, while that of the β-phase were identified as 840, 884, and 1279 cm^{-1} [31]. The lines indicating the position of these bands in the four samples are shown in Fig. 5. Overall, it is noticed from the figure that when each BTO and UAC individually act as filler, each can contribute to the nucleation of the β-phase. However, BTO shows better nucleating power than UAC as can be seen from the spectra of samples A and B, which agrees with the observations in [20]. Furthermore, it is observed that both samples B and H exhibit a very close trend within certain absorption bands, but overall the peaks of the spectra for sample H outperform that of sample B.

Fig. 6 reveals the β-phase content in all solution-cast samples. To calculate the relative fraction of the β-phase content, we employed the Beer-Lambert Law [31]:

$$F(\beta) = \frac{A_\beta}{(\frac{K_\beta}{K_\alpha})A_\alpha + A_\beta} \quad (1)$$

where A_β and A_α symbolize the absorbance at $766cm^{-1}$ and $840cm^{-1}$, respectively. Besides, the parameters K_α and K_β denote the absorption coefficients at the above corresponding wavenum-

Table 3
Variation of printing factors.

Factors		Levels		
		1	2	3
A	Printing bed temperature	50℃	75℃	95℃
B	Printing speed	$10mm/s$	$15mm/s$	$25mm/s$

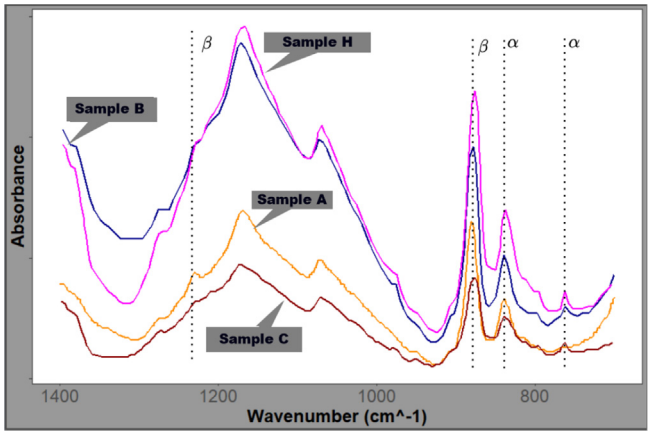

Fig. 5. Annotated FTIR spectra of samples A, B, C, and H.

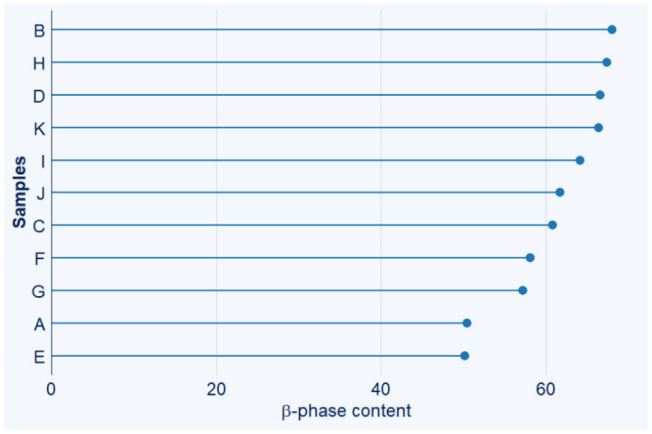

Fig. 6. Variation of the β-phase content for all solution-cast samples.

ber, and each takes the value of $6.1 \times 10^4 cm^2 mol^{-1}$ and $7.7 \times 10^4 cm^2 mol^{-1}$, respectively [33]. Employing Eq. (1), Fig. 6 reveals that sample A, which contains PVDF-HFP (98 wt%) and UAC (2 wt%) yield the lowest β-phase content (50.4%). In contrast, sample B produces the highest β-phase content (68.12%), followed by sample H with a β-phase content of 67%. For context, Wu *et al* [34] obtained a β-phase content of 72 % with only carbon black at 0.5 wt% loading of PVDF-HFP after poling. Moreover, Kim et al [20] reported the highest β-phase content of 55.91% with 15*wt*% of BTO alone (before poling). However, as it would be shown in the coming paragraph, controlling the 3D printing parameter paved the way for even further enhancement of the β-phase content.

Now, although sample B yield a higher β-phase fraction than sample H, the FTIR spectra in Fig. 5 indicates that sample H (10.55 wt% BTO and 0.45 wt% UAC) produces the more prominent higher peaks of the β-phase absorption band. For this reason, a composite gel derived from the solution mixture of sample H (rather than B) was prepared for onward use with the syringe-based FDM platform. A nozzle diameter of 400μm ais employed. The FDM 3D printing is done to examine the effect of printing parameters on the proportion of the β-phase. After the printing process, the FDM-produced samples were further annealed at 95 °C for 5 h, inspired by [29]. Analysis of the β-phase content of the FDM-produced samples with the factor variations highlighted in Table 3 yield Fig. 7. It is observed from this plot that higher printing bed temperature and lower printing speed favour a higher β-phase content. Indeed, a β-phase content of 79.6% is obtained for specimen fabricated at 95℃ and 10*mm*/*s*. Technically, this can be attributed to the fact that higher temperature facilitates faster evaporation of the remnant solvent in the mixture, while the low speed favours consistent drawing of the gel, both of which aid the crystallization process [35]. In all, the mean, median and upper quartile of the samples produced at 95℃ exceeds those at the other two temperature values. Besides, the increased β-phase content here translates to enhanced piezoelectric response without poling and can be further linked to the combined effect of the extrusion

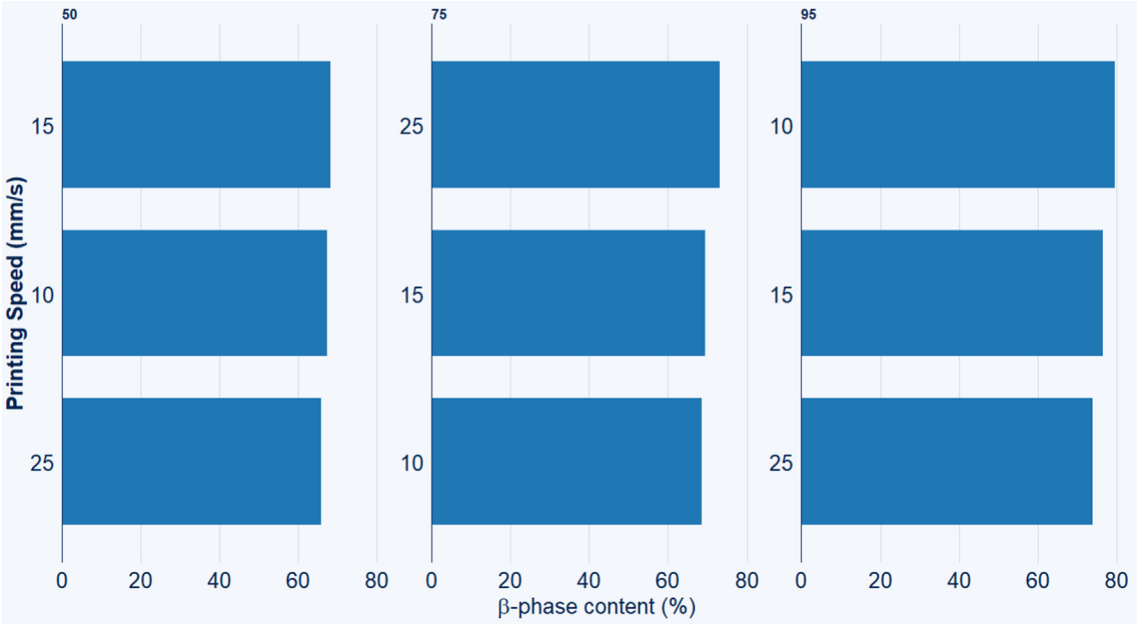

Fig. 7. Variation of the β-phase content with printing parameters.

Table 4
Experimental results of the pressure sensing test.

Pressure (Kg/cm^2)	Voltage (mV)
1.50	0.78
2.00	1.43
2.50	3.12
3.00	5.87
3.50	6.29
4.00	7.91
4.50	8.36

pressure and thermal annealing experienced by the samples during the preparation [21,36]. Put together, the results suggest that the prudent use of the printing bed temperature and the post-fabrication annealing can both help to further improve the crystallinity of the FDM-produced samples. Although the syringe-based FDM is used for the results presented here, this observation supports the use of thermal annealing to improve the mechanical properties of extruder-based FDM-produced parts [37]. Combined with the flexibility of the FDM process to produce complex 3D structured parts, these conditions are expected to ease the production of piezo-responsive structures with more complicated profiles than simple planar structures that can be obtained with solution casting, which is generally considered to be a low-yield, time-consuming process as demonstrated by Bodkhe et al [21]. As a final step, the electromechanical response of the strips produced via the optimal 3D printing conditions was conducted in terms of the pressure-voltage relationship. Table 4 contains the compilation of the experimental tests on pressure sensing test of unpoled PVDF-HFP-UAC composite strips of thickness 0.5*mm*, length of 40*mm* and width of 10*mm*.

4. Conclusion

One of the technical hindrances to the proliferation of piezoelectric polymers is the constraint imposed by the current production methods that favour mostly the fabrication of small-scale planar samples but faced challenges in producing piezoelectric devices of sufficient complexity and a wider working area. The present study was designed to evaluate the combined influences of $BaTiO_3$ (BTO) and untreated activated carbon (UAC) as fillers and FDM printing conditions on the piezoelectric response of PVDF-HFP, a copolymer of PVDF. Towards this goal, solution-cast composite samples of the PVDF-HFP with BTO and UAC in various weight fractions were produced based on the extreme vertices type of design of experiment . The characterization of the solution-cast samples was achieved with FTIR, revealing the vibrational spectra and the β-phase fractions contained in the samples. The composite consisting of 10.55 BTO wt% and 0.45 wt% UAC within the matrix of PVDF-HFP was found to yield a 67 % proportion of the piezoelectric β-phase content. Further employed for the syringe-based FDM process, the composite gel of this high-performing PVDF-HFP-BTO-UAC combination is observed to further undergo additional phase transformation nucleation with an increased β-phase content under the combined effect of high bed temperature, low printing speed and post-fabrication annealing. With the flexibility of the produced strips still intact after 3D printing, the current effort lays the groundwork for future research on more complex flexible piezoelectric structures for use in wearable pressure sensing applications.

Data availability

Data will be made available on request.

Declaration of Competing Interest

The authors declare that they have no known competing financial interests or personal relationships that could have appeared to influence the work reported in this paper.

Acknowledgments

This work was supported by Malaysia's Ministry of Education (MOE) under the Fundamental Research Grant Scheme (FRGS/1/2018/TK03/UNIM/02/1). The first author also acknowledges the 2022 FOSE staff support.

"I, Khameel B Mustapha, the Corresponding Author, declare that this manuscript is original, has not been published before and is not currently being considered for publication elsewhere.

I can confirm that the manuscript has been read and approved by all named authors and that there are no other persons who satisfied the criteria for authorship but are not listed. I further confirm that the order of authors listed in the manuscript has been approved by all of us.

I understand that the Corresponding Author is the sole contact for the Editorial process and is responsible for communicating with the other authors about progress, submissions of revisions and final approval of proofs.

Signed by Khameel B Mustapha on behalf of the all other authors"

References

[1] J. Gardan, Smart materials in additive manufacturing: state of the art and trends, Virtual and physical prototyping 14 (1) (2019) 1–18.
[2] K. Mustapha, K.M. Metwalli, A review of fused deposition modelling for 3D printing of smart polymeric materials and composites, Eur. Polym. J. 156 (2021) 110591.
[3] J.-Y. Lee, J. An, C.K. Chua, Fundamentals and applications of 3D printing for novel materials, Appl. Mater. Today 7 (2017) 120–133.
[4] J. Ahn, J. Gu, J. Choi, C. Han, Y. Jeong, J. Park, S. Cho, Y.S. Oh, J.H. Jeong, M. Amjadi, A Review of Recent Advances in Electrically Driven Polymer-Based Flexible Actuators, *Smart Materials, Structures, and Their Applications.* Advanced Materials Technologies (2022) 2200041.
[5] Z.X. Khoo, J.E.M. Teoh, Y. Liu, C.K. Chua, S. Yang, J. An, K.F. Leong, W.Y. Yeong, 3D printing of smart materials: A review on recent progresses in 4D printing, Virtual and Physical Prototyping 10 (3) (2015) 103–122.
[6] F. Momeni, X. Liu, J. Ni, A review of 4D printing, Mater. Des. 122 (2017) 42–79.
[7] S.C. Ligon, R. Liska, J. Stampfl, M. Gurr, R. Mülhaupt, Polymers for 3D printing and customized additive manufacturing, Chem. Rev. 117 (15) (2017) 10212–10290.
[8] Gibson, I., D.W. Rosen, and B. Stucker, *Additive manufacturing technologies*. Vol. 17. 2014: Springer.
[9] S.C. Daminabo, S. Goel, S.A. Grammatikos, H.Y. Nezhad, V.K. Thakur, Fused deposition modeling-based additive manufacturing (3D printing): techniques for polymer material systems, Mater. Today Chem. 16 (2020) 100248.
[10] M. Nadgorny, A. Ameli, Functional polymers and nanocomposites for 3D printing of smart structures and devices, ACS Appl. Mater. Interfaces 10 (21) (2018) 17489–17507.
[11] K.R. Ryan, M.P. Down, C.E. Banks, Future of additive manufacturing: Overview of 4D and 3D printed smart and advanced materials and their applications, Chem. Eng. J. 403 (2021) 126162.
[12] C. Lee, J.A. Tarbutton, Electric Poling-assisted Additive Manufacturing Process for Lead-free Piezoelectric Device Fabrication, Procedia Manuf. 1 (2015) 320–326.
[13] C. Lee, J.A. Tarbutton, Electric poling-assisted additive manufacturing process for PVDF polymer-based piezoelectric device applications, Smart Mater. Struct. 23 (9) (2014) 095044.
[14] D.A. Porter, T.V.T. Hoang, T.A. Berfield, Effects of in-situ poling and process parameters on fused filament fabrication printed PVDF sheet mechanical and electrical properties, Addit. Manuf. 13 (2017) 81–92.
[15] N. Momenzadeh, H. Miyanaji, D.A. Porter, T.A. Berfield, Polyvinylidene fluoride (PVDF) as a feedstock for material extrusion additive manufacturing, Rapid Prototyping Journal (2020).
[16] J. Fan, D. Gonzalez, J. Garcia, B. Newell, R.A. Nawrocki, The Effects of Additive Manufacturing and Electric Poling Techniques on PVdF Thin Films: Towards 3D Printed Functional Materials, Smart Materials, Adaptive Structures and Intelligent Systems, American Society of Mechanical Engineers, 2020.
[17] C. Lee, J.A. Tarbutton, Polyvinylidene fluoride (PVDF) direct printing for sensors and actuators, The International Journal of Advanced Manufacturing Technology 104 (5) (2019) 3155–3162.

[18] Asadi, K., *Organic Ferroelectric Materials and Applications*. 2021: Elsevier.
[19] C. Eshwar Reddy, *A Review on 3D printing of piezoelectric materials.* IOP Conference Series, Materials Science and Engineering 455 (1) (2018).
[20] H. Kim, F. Torres, D. Villagran, C. Stewart, Y. Lin, T.L.B. Tseng, 3D printing of BaTiO3/PVDF composites with electric in situ poling for pressure sensor applications, Macromol. Mater. Eng. 302 (11) (2017) 1700229.
[21] S. Bodkhe, G. Turcot, F.P. Gosselin, D. Therriault, One-step solvent evaporation-assisted 3D printing of piezoelectric PVDF nanocomposite structures, ACS Appl. Mater. Interfaces 9 (24) (2017) 20833–20842.
[22] R. Kumar, R. Singh, M. Singh, P. Kumar, On ZnO nano particle reinforced PVDF composite materials for 3D printing of biomedical sensors, J. Manuf. Processes 60 (2020) 268–282.
[23] Sharma, R., R. Singh, and A. Batish, *On effect of chemical-assisted mechanical blending of barium titanate and graphene in PVDF for 3D printing applications.* Journal of Thermoplastic Composite Materials. **0**(0): p. 0892705720945377.
[24] N.A. Shepelin, V.C. Lussini, P.J. Fox, G.W. Dicinoski, A.M. Glushenkov, J.G. Shapter, A.V. Ellis, 3D printing of poly(vinylidene fluoride-trifluoroethylene): a poling-free technique to manufacture flexible and transparent piezoelectric generators, MRS Commun. 9 (1) (2019) 159–164.
[25] X. Yuan, X. Gao, X. Shen, J. Yang, Z. Li, S. Dong, A 3D-printed, alternatively tilt-polarized PVDF-TrFE polymer with enhanced piezoelectric effect for self-powered sensor application, Nano Energy 85 (2021) 105985.
[26] M. Marandi, J. Tarbutton, Additive manufacturing of single-and double-layer piezoelectric PVDF-TrFE copolymer sensors, Procedia Manuf. 34 (2019) 666–671.
[27] A. Ikei, J. Wissman, K. Sampath, G. Yesner, S.N. Qadri, Tunable In Situ 3D-Printed PVDF-TrFE Piezoelectric Arrays, Sensors 21 (15) (2021) 5032.
[28] M. Aldas, G. Boiteux, G. Seytre, Z. Ghallabi, Dielectric Behaviour of BaTiO 3/P (VDF-HFP) Composite Thin Films Prepared by Solvent Evaporation Method, IEEE, 2010.
[29] S. Satapathy, P. Gupta, S. Pawar, and K. Varma, *Crystallization of Beta-phase Poly (vinylidene fluoride) films using dimethyl sulfoxide (DMSO) solvent and at suitable annealing condition.* arXiv preprint arXiv:0808.0419, 2008.
[30] M.J. Anderson, P.J. Whitcomb, Mixture DOE uncovers formulations quicker, Rubber and Plastics News (2002) 16–18.
[31] P. Martins, A. Lopes, S. Lanceros-Mendez, Electroactive phases of poly (vinylidene fluoride): Determination, processing and applications, Prog. Polym. Sci. 39 (4) (2014) 683–706.
[32] T. Roopaa, H.N. Murthy, V.P. Kumar, M. Krishna, Development and Characterization of PVDF Thin Films for pressure sensors, Mater. Today:. Proc. 5 (10) (2018) 21082–21090.
[33] V. Sencadas, R. Gregorio Jr, S. Lanceros-Méndez, α to β phase transformation and microestructural changes of PVDF films induced by uniaxial stretch, J. Macromol. Sci. 48 (3) (2009) 514–525.
[34] L. Wu, W. Yuan, N. Hu, Z. Wang, C. Chen, J. Qiu, J. Ying, Y. Li, Improved piezoelectricity of PVDF-HFP/carbon black composite films, J. Phys. D Appl. Phys. 47 (13) (2014) 135302.
[35] J. Gregorio, Rinaldo and M. Cestari,, Effect of crystallization temperature on the crystalline phase content and morphology of poly (vinylidene fluoride), J. Polym. Sci., Part B: Polym. Phys. 32 (5) (1994) 859–870.
[36] J.H. Park, N. Kurra, M. AlMadhoun, I.N. Odeh, H.N. Alshareef, A two-step annealing process for enhancing the ferroelectric properties of poly (vinylidene fluoride)(PVDF) devices, J. Mater. Chem. C 3 (10) (2015) 2366–2370.
[37] R.A. Wach, P. Wolszczak, A. Adamus-Wlodarczyk, Enhancement of mechanical properties of FDM-PLA parts via thermal annealing, Macromol. Mater. Eng. 303 (9) (2018) 1800169.